

Source Aware Deep Learning Framework for Hand Kinematic Reconstruction using EEG Signal

Sidharth Pancholi, *Member, IEEE*, Amita Giri, *Student Member, IEEE*, Anant Jain, *Student Member, IEEE*, Lalan Kumar, *Member, IEEE*, and Sitikantha Roy, *Member, IEEE*

Abstract—The ability to reconstruct the kinematic parameters of hand movement using non-invasive electroencephalography (EEG) is essential for strength and endurance augmentation using exosuit/exoskeleton. For system development, the conventional classification based brain computer interface (BCI) controls external devices by providing discrete control signals to the actuator. A continuous kinematic reconstruction from EEG signal is better suited for practical BCI applications. The state-of-the-art multi-variable linear regression (mLR) method provides a continuous estimate of hand kinematics, achieving maximum correlation of upto 0.67 between the measured and the estimated hand trajectory. In this work, three novel source aware deep learning models are proposed for motion trajectory prediction (MTP). In particular, multi layer perceptron (MLP), convolutional neural network - long short term memory (CNN-LSTM), and wavelet packet decomposition (WPD) CNN-LSTM are presented. Additional novelty of the work includes utilization of brain source localization (using sLORETA) for the reliable decoding of motor intention mapping (channel selection) and accurate EEG time segment selection. Performance of the proposed models are compared with the traditionally utilised mLR technique on the real grasp and lift (GAL) dataset. Effectiveness of the proposed framework is established using the Pearson correlation coefficient and trajectory analysis. A significant improvement in the correlation coefficient is observed when compared with state-of-the-art mLR model. Our work bridges the gap between the control and the actuator block, enabling real time BCI implementation.

Index Terms—BCI, Deep Learning, EEG, Intention Mapping, Motion Trajectory Prediction, Non-Invasive, Source Localization.

I. INTRODUCTION

Electroencephalography (EEG) signal has been extensively utilized for brain computer interface (BCI) applications because of its high temporal resolution, non-invasive nature, portability, and cost-effectiveness [1]–[5]. BCI systems facilitates direct connection between the brain and external devices that do not rely on the peripheral nerves and muscles.

Hence, BCI based devices like wearable robots [4], [6], exoskeletons [5], [7], [8], and prosthesis [9] have gained focus

This work was supported in part by Prime Minister's Research Fellowship (PMRF), Ministry of Human Resource Development (MHRD), GoI, with project number PLN08/PMRF (to A. Giri) and in part by DRDO - IITD 'JATC' with project number RP03830G.

S. Pancholi, A. Giri and A. Jain are with the Department of Electrical Engineering, Indian Institute of Technology, Delhi, India (e-mail: s.pancholi@ieee.org; Amita.Giri@ee.iitd.ac.in; anantjain@ee.iitd.ac.in)

L. Kumar is with the Department of Electrical Engineering and Bharti School of Telecommunication, Indian Institute of Technology, Delhi, India (e-mail: lkumar@ee.iitd.ac.in)

S. Roy is with the Department of Applied Mechanics, Indian Institute of Technology, Delhi, India (e-mail: sroy@am.iitd.ac.in)

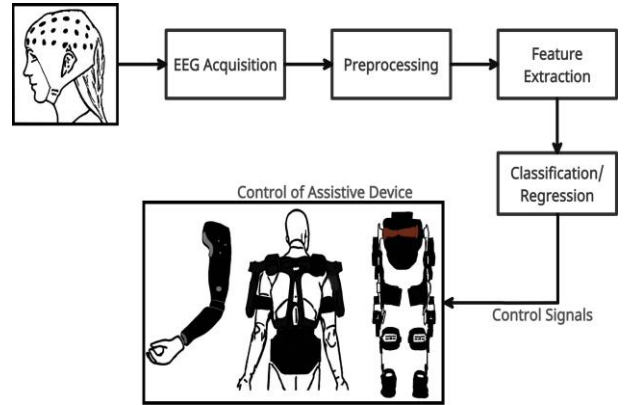


Fig. 1: Schematic diagram of EEG signal based BCI system.

in the recent years. When such external devices are utilized for strength and endurance augmentation, reconstruction of motion trajectory kinematic parameters from EEG signal becomes important. Reliable decoding of motor intentions and accurate timing of the robotic device actuation is fundamental to optimally enhance the subject's functional improvement. Since, EEG signal has information about the kinematic parameters prior to the actual movement, this time gain along with correct intention mapping will facilitate the real time control of assistive devices. A schematic diagram of EEG signal based BCI systems is shown in the Fig. 1.

Multi-class classification [10], [11] and regression [12] are the two major approaches adopted in EEG based BCI control. Multi-class classification based BCI systems utilize feature extraction and classification method to maximize the inter-class variance and realize decisive planes that separate distinct classes [13]. However, regression-based techniques provide more natural control of assistive devices through continuous decoding of EEG signal. Brain activity recorded as EEG signal, exhibits non-stationary nature and therefore requires continuous estimation of optimal and stationary features from the signal. Motion trajectory prediction (MTP) from multi-channel EEG signals was proposed in [12] using the multi-variate linear regression (mLR) technique. In particular, Kalman filter based mLR model was utilized to decode 2D hand movement in the horizontal plane. Mean correlation value of 0.60 ± 0.07 was achieved between the predicted and the measured trajectory. The most adopted hand crafted feature for regression is power spectral density (PSD) from the four frequency bands that include delta (1-3Hz), theta (5-8Hz),

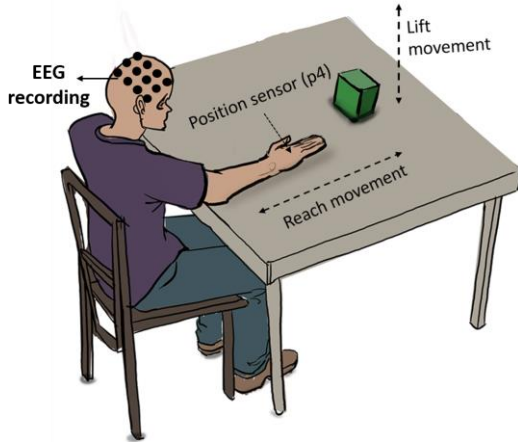


Fig. 2: Experimental set-up of reach to grasp movement.

alpha (9-12Hz), and beta (14-31Hz) [14]. In [15], decoding of 3D imagined hand movement trajectory was studied using PSD based band-power time series (BTS) technique. A significant improvement in accuracy was observed using BTS input when compared with the standard potentials time-series (PTS) input. The most recent work [16], demonstrated the feasibility of predicting both actual and imagined 3D trajectories of all arm joints from scalp EEG signals using mLR model.

In the past few years, deep learning a subfield of machine learning has achieved breakthrough accuracies in complex and high dimensional data such as image classification [17], emotion recognition [18], and machine translation [19]. Deep learning focuses on computational models that typically learn hierarchical representations of the input data through successive non-linear transformations—termed neural networks. The convolutional neural network (CNN/ConvNet) has been extensively utilized for BCI applications that include motor imagery (MI) and motor execution (ME) classification [20]. The widespread use of CNN algorithms in classification application [21], [22] is due to its capability to extract spatial information from EEG signal. However, it intrinsically disregards the temporal information [23]. A very widely known recurrent neural network which effectively utilizes the temporal dependencies based on past information is long short-term memory (LSTM) network [24].

In this work, a basic feed forward neural network called multi layer perceptron (MLP) along with CNN-LSTM based hybrid deep learning framework is proposed for hand kinematics prediction. To the best of authors' knowledge, CNN itself has not been utilized for MTP. Reconstruction of hand movement profiles using low frequency EEG have been reported in 2D [25] and 3D spaces [26]. These results indicate that detailed limb kinematic information could be present in the low frequency components of EEG, and could be decoded using the proposed models. Hence, an advanced version of CNN-LSTM based on wavelet packet decomposition (WPD) is proposed that decompose the EEG signal into sub-bands with increasing resolution towards the lower frequency band [27], [28]. Additional novelty of the work includes utilization of brain source localization (BSL) for the reliable decoding of motor intention mapping (channel selection) and accurate EEG

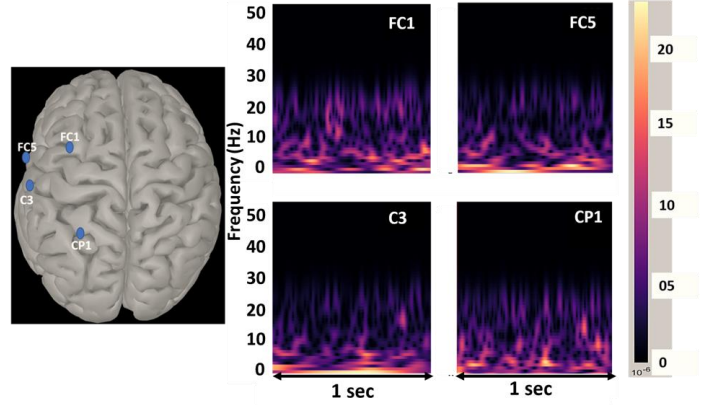


Fig. 3: Time-frequency distribution of FC1, FC5, C3, and CP1 EEG channels.

time segment selection. Electrodes placed over the active brain region corresponding to the hand movement are utilized, rather than all the available sensors data for efficient computation. The EEG segment is selected accordingly and utilized in the training and testing of the model.

The rest of the paper is organized as follows. The details of the experimental data and signal pre-processing steps are covered in Section II. The description of existing state-of-the-art model is presented in Section III. The three proposed source aware deep learning models along with the role of brain source localization in MTP is presented in Section IV. Performance evaluation metric is reported in Section V. Section VI concludes the paper.

II. EXPERIMENTAL DATA AND PRE-PROCESSING

In this work, WAY-EEG-GAL (Wearable interfaces for hAnd function recoverY- EEG - grasp and lift) data-set [29] is utilized for MTP. Scalp EEG recordings were collected from twelve healthy subjects for right hand movement. In this experiment, the task to be executed was to reach and grasp the object and lift it stably for a couple of seconds. The participant can then lower the object at its initial position and retract the arm back to resting position. The data acquisition set up for the same is illustrated in Fig. 2. A series of such reach to grasp and lift trials were executed for various loads and surface frictions. The beginning of the task and lowering of the object was cued by an LED. The kinematic data was obtained using a position sensor p4 (as shown in Fig. 2) normalized between 0 to 1 with initial position as 0 and maximum as 1. This was done to get rid of error due to initial position perturbation. Trials with delay up to 700ms between the LED cue and the actual movement is considered. The trials in which the response time is more than 700ms have been excluded from this study. The pre-processing steps followed is detailed next.

The kinematics and EEG data were down sampled from 500 Hz to 100 Hz. The time-frequency distribution of EEG signal for a particular subject is shown in the Fig. 3 for FC1, FC5, C3, and CP1 channel. It may be noted that the maximum power related to right hand movement is present in the delta (0.5-3 Hz), theta (3-7 Hz), and lower alpha (7-12 Hz) range. Hence,

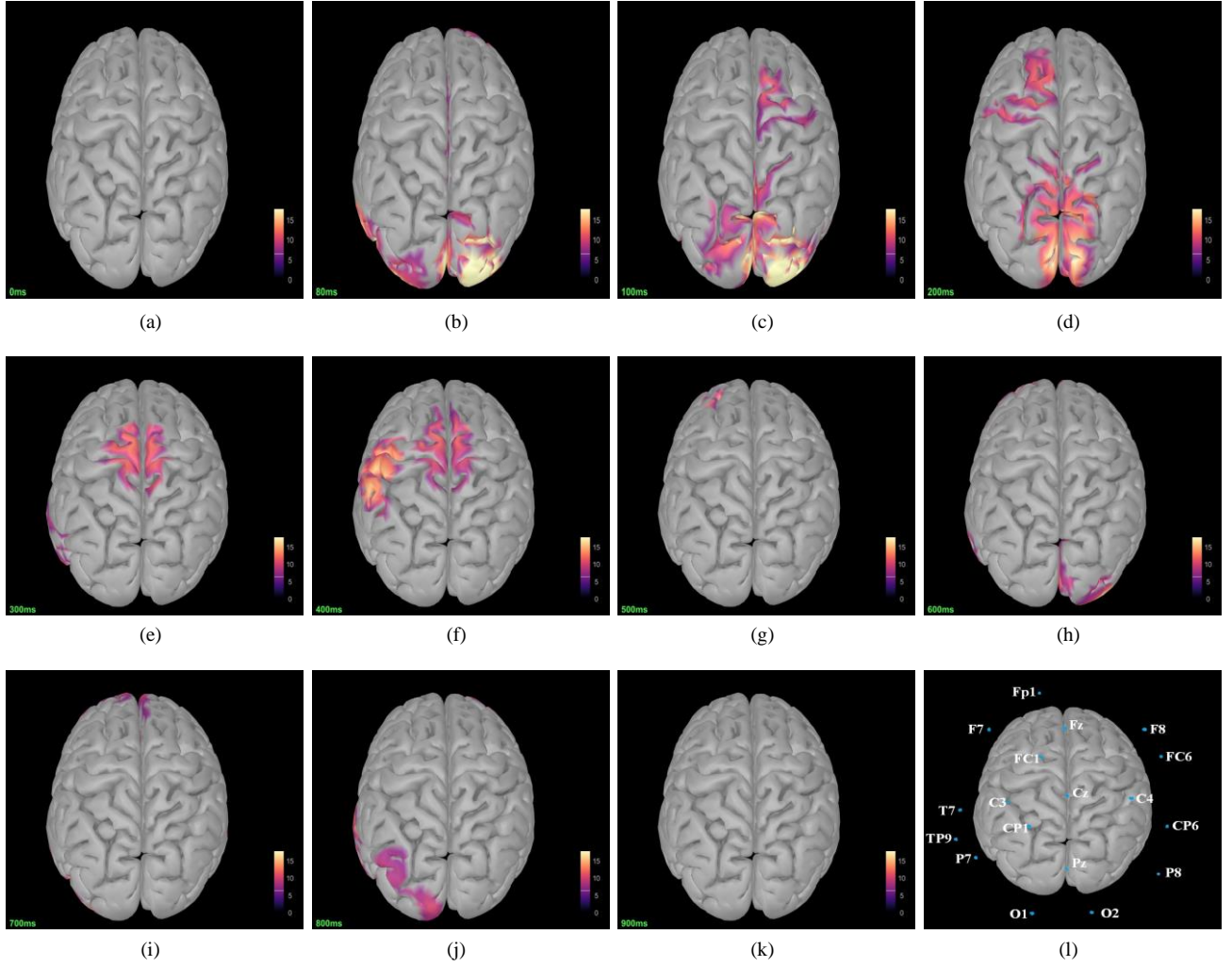


Fig. 4: Brain source localization using sLORETA at different time stamps : (a) 0ms (b) 80ms (c) 100ms (d) 200ms (e) 300ms (f) 400ms (g) 500ms (h) 600ms (i) 700ms (j) 800ms (k) 900ms. (l) Selected 18 channels of maximum activity using BSL.

the EEG time series was first filtered using zero-phase 4th order Hamming-windowed sinc FIR (finite impulse response) filter in the range of delta, theta, and lower alpha bands. Subsequently, ICA algorithm was applied to remove artifacts such as eye movement, eye blink, and power line interference. The common average referencing method was used for re-referencing. The EEG signal was finally standardized as

$$V_n[t] = \frac{v_n[t] - \bar{v}_n}{\sigma_n} \quad (1)$$

where $V_n[t]$ is the standardized EEG voltage at time t and at sensor n . There are total N number of EEG electrodes. The mean and standard deviation of v_n is represented by \bar{v}_n and σ_n respectively.

III. THE EXISTING MLR MODEL FOR KINEMATIC DECODING

Multi-variate linear regression has been the state-of-the-art technique for MTP based BCI [12], [16], [26]. In this section, application of mLR in mapping the EEG time series signal to the kinematic parameters in continuous manner, is briefly

detailed. The mLR equations for the mapping are as follows [26].

$$\begin{aligned} \sum_{n=1}^N \sum_{l=0}^L P_x[t] &= a_x + \sum_{n=1}^N \sum_{l=0}^L b_x^{(nl)} V_n[t-l] \\ P_y[t] &= a_y + \sum_{n=1}^N \sum_{l=0}^L b_y^{(nl)} V_n[t-l] \end{aligned} \quad (3)$$

$$P_z[t] = a_z + \sum_{n=1}^N \sum_{l=0}^L b_z^{(nl)} V_n[t-l] \quad (4)$$

Here, $P_x[t]$, $P_y[t]$, and $P_z[t]$ are the horizontal, vertical, and depth positions of the hand at time sample t , respectively. $V_n[t-l]$ is the standardized voltage at time lag l , where the number of time lags is varied from 0 to L . The regression coefficient a and b are estimated by minimizing the loss function during the training phase. In mLR, the multiple independent variables ($V_n[t-l]$) contribute to a dependent kinematic variable ($P_x[t]$, $P_y[t]$, and $P_z[t]$).

IV. SOURCE AWARE DEEP LEARNING MODELS FOR HAND KINEMATIC RECONSTRUCTION

In this Section, source aware deep learning models for hand kinematic reconstruction are proposed. In particular, MLP, CNN-LSTM and WPD CNN-LSTM are proposed for the kinematic parameter estimation. As the kinematic movement is embedded in the EEG signature, early detection of intended movement is essential for controlling an external BCI devices for positive real time augmentation. Source localization plays a key role in motor intention mapping (channel selection) and accurate EEG time segment selection. Hence, role of brain source localization on MTP is detailed first followed by the model description.

A. Role of Brain Source Localization in MTP

Brain source localization refers to the estimation of active dipole location from noninvasive scalp measurements. It is an ill-posed inverse problem, where the relationship between the EEG scalp potential and neural sources is non-unique, and the solution is highly sensitive to the artifacts. Dipole-fitting and dipole imaging (distributed source model) are two approaches to solve the inverse problem. In the dipole fitting method, small number of active regions are considered in the brain and can be modeled using equivalent dipoles [30], [31]. The dipole fitting is an over-determined approach to BSL and is solved using a nonlinear optimization technique. This includes subspace-based multiple signal classification (MUSIC) [32], [33], beamforming [34], and genetic [35] algorithms. On the other hand, the distributed source model assumes that there are a large number of sources confined in an active region of the brain and is solved using linear optimization techniques, such as minimum norm estimation (MNE) [36], weighted MNE (WMNE) [37], low resolution electromagnetic tomography (LORETA) [38], and standardized low resolution brain electromagnetic tomography (sLORETA) [39]. EEG signals have been found to be effective for monitoring changes in the human brain state and behavior [40].

In the present work, sLORETA dipole imaging method is opted for the inverse source localization. In this method, localization inference is performed using images of standardized current density under the constraint of smoothly distributed sources. Source localization plots for the activity under consideration (right hand grasp and lift execution task) are given in Fig. 4. There are total 11 images of cortical surface activation sliced temporally. The result shown corresponds to single trial EEG of the subject 3 and is reproducible for the other trials as well. Visual cue for the start of the activity was presented at 0ms. It may be noted that the brain region responsible for visual processing (occipital lobe) shows neural activation after 80-120ms of the visual cue (Fig. 4(b)-(c)). Prompted hand movement information was transferred to the sensory motor region at around 280-300ms (Fig. 4(e)). In response to right hand movement, contralateral motor cortex i.e. left motor cortex gets elucidated at 350-400ms (Fig. 4(f)). No motor related neural activity is noticed thereafter (Fig. 4(g)-(k)). It was observed that the Subject actually performed hand movement at 620-650ms after the cue was shown. Hence, it may be concluded

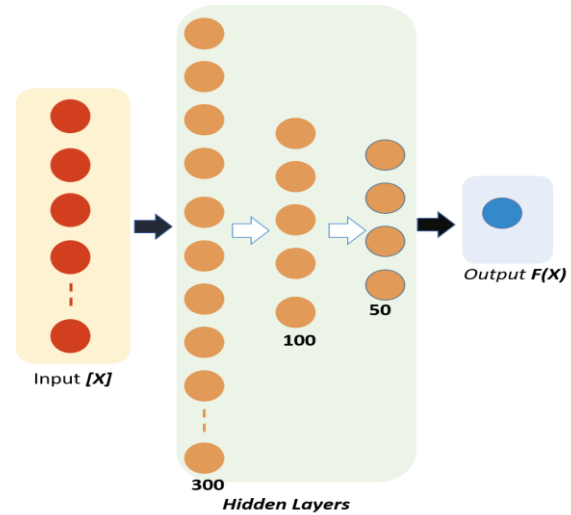


Fig. 5: Multi-layer perceptron based regression modeling

that the EEG source localization can provide the intended hand movement information approximately 300ms prior to the actual hand movement.

Early detection of intended hand movement is essential in communicating or controlling an external BCI devices. Therefore, the EEG time segment was taken 300ms prior to the actual hand movement. The length of the EEG and kinematic data were made equal by removing the EEG samples from the end of a trial. The EEG segment was selected accordingly and utilized in the training and testing of the proposed model. In addition to that, electrodes placed over the maximal neural activation region corresponding to the hand movement were utilized. In particular, electrodes on the left hemisphere (Fp1, F7, FC1, T7, C3, TP9, CP1, P7, O1), near the midline (Fz, Cz, Pz) and on the right hemisphere (F8, FC6, C4, CP6, P8, O2) were utilised as shown in Fig. 4(l). Hence, rather than using all the 32 EEG channels for kinematics reconstruction, only 18 channels of maximum activity were chosen. Brain source localization facilitates the reliable decoding of motor intention mapping (channel selection) and accurate EEG time segment selection.

B. Model I : Multi-layer Perceptron Model based

Deep learning based models are not much explored in the literature for MTP using EEG signal. However, MLP has been utilized for EEG classification [41]. Multi-layer perceptron is first proposed herein for trajectory prediction using EEG signal. The model is illustrated in the Fig.5. The building blocks of a neural networks are neurons (or perceptron), weights and activation functions. For activation function, rectified linear unit (ReLU) is employed herein and is defined as

$$F(\Omega) = \max(0, \Omega) \quad (5)$$

where Ω is the input parameter to the activation function F . The MLP model utilizes a feed-forward neural network consisting of input, hidden and output layers. In particular, there are 3 hidden layers having 300, 100 and 50 perceptrons,

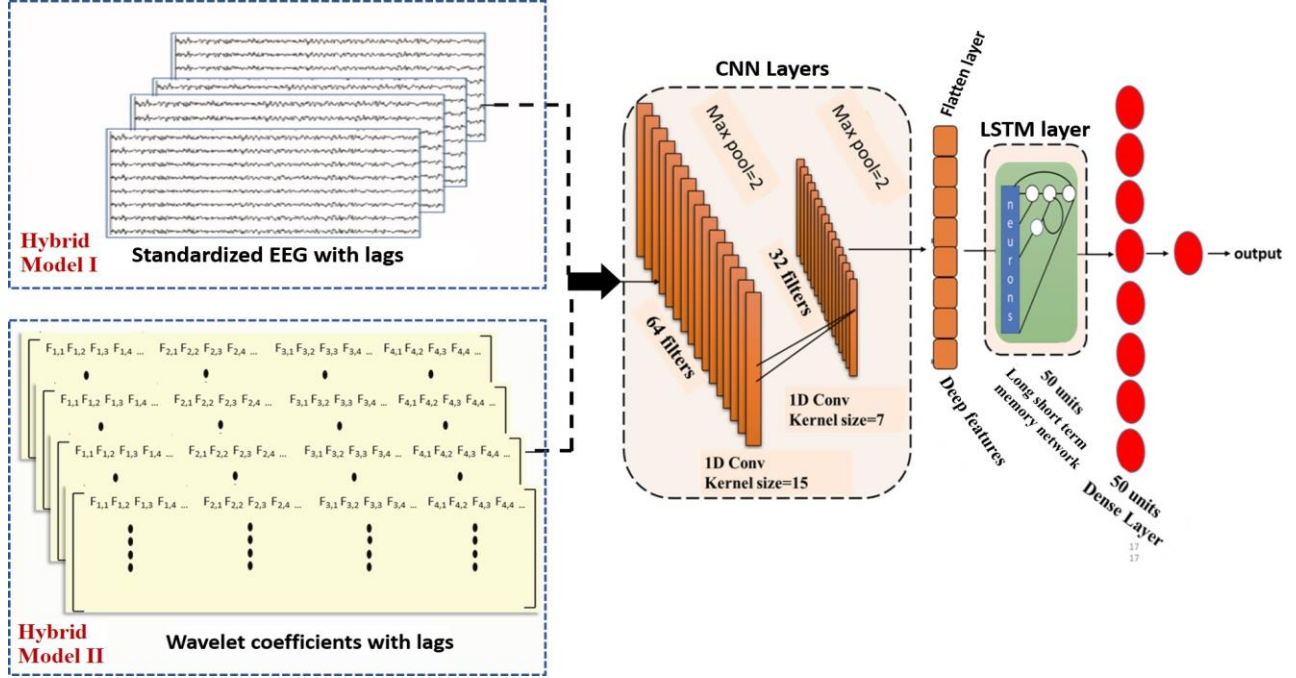


Fig. 6: Proposed source aware hybrid model I utilizes EEG time series as an input and hybrid model II takes wavelet coefficients for predicting the kinematics of upper limb.

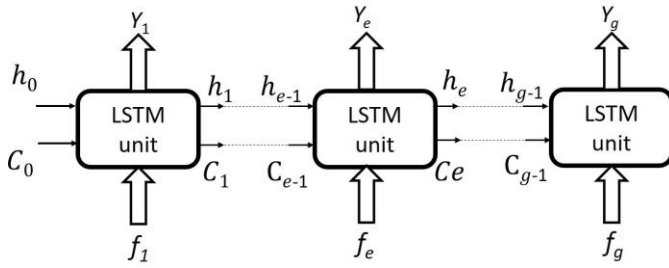


Fig. 7: Unfold structure of LSTM network.

in addition to input and output layer. The output of the d th neuron at the first hidden layer is given by

$$h_d^1 = F(b_d^1 + \sum_{i=1}^{D_0} u_{i,d}^0 V_i), \quad d = 1, \dots, D_1 \quad (6)$$

where b_d^1 is the input bias, D_0 is the size of input vector and D_1 represents the total number of neuron at first hidden layer. $u_{i,d}^0$ is the weight between the i th element of the input V_i to the d th neuron at the first hidden layer. Since, every perceptron in each layer of the neural network is connected to every other perceptron in the adjacent layer. The output of the d th neuron at k th hidden layer can now be expressed as

$$h_d^k = F(b_d^k + \sum_{i=1}^{D_{k-1}} u_{i,d}^{k-1} h_i^{k-1}), \quad d = 1, \dots, D_k, \quad (7)$$

where $k = 2, \dots, K$ represents the hidden layer with a total of K hidden layers. $u_{i,d}^{k-1}$ is the weight between the i th neuron in the $(k-1)$ th hidden layer to the d th neuron at the k th

hidden layer. The neural network weights are updated using the Adam optimizer. The output of the k th hidden layer can be expressed as

$$h^k = [h_1^k \ h_2^k \ \dots \ h_{D_k}^k]^T \quad (8)$$

The output layer y of the model yields the desired kinematic parameters. The j th element of the output is given by

$$y_j = F(b_j + \sum_{i=1}^{D_k} w_{i,j}^K h_i^K) \quad (9)$$

where b_j is the output bias.

C. Hybrid Model I : CNN-LSTM based

In this Section, a hybrid deep learning based model is proposed for MTP on the GAL dataset. In particular, CNN and LSTM [42] based deep learning model along with a dense layer is utilized and is shown in Fig. 6. Hybrid model I utilizes the pre-processed EEG with time lag $L = 10$. The CNN algorithm is seen to be useful for feature engineering/extraction through layer-by-layer processing [43]. The

proposed model makes use of CNN to extract inherent spatial information present in EEG time series. More specifically, relevant combination of sensors is extracted.

The proposed CNN architecture consists of two 1D convolutional layers with 64 and 32 filters having kernel size of 15 and 7 respectively. The 1D forward propagation (1D-FP) for the d th neuron of the k th CNN layer is expressed as

$$Z_d^k = q_d^k + \sum_{i=1}^{D_{k-1}} \text{conv1D}(J_{i,d}^{k-1}, S_i^{k-1}) \quad (10)$$

where q_d^k is the bias, D_{k-1} is the total number of neuron at layer $k-1$ and $conv1D$ represents the one dimensional convolution. The $J_{i,d}^{k-1}$ denotes the kernel from the i th neuron at layer $k-1$ to the d th neuron at layer k . The output of i th neuron at $(k-1)$ th layer is represented by S_i^{k-1} . Intermediate output feature is now given by

$$y_d^k = F(Z_d^k) \quad (11)$$

where y_d^k represents output of d th neuron at layer k . A max-pooling layer for sub-sampling is employed between the two layers.

Output of the CNN module is fed to the flatten layer for generating the intermediate deep features. The deep features are in turn, input to the LSTM layer. Total 50 cells are used in the LSTM layer for creating enhanced temporal features. The structure of LSTM network for an input feature sequence $[f_1, f_2, \dots, f_g]$ is illustrated in the Fig. 7. The hidden state h_e and activation vector c_e at time-step ($e = 1, 2, \dots, g$). The LSTM unit utilizes the past state h_{e-1} , c_{e-1} and current state features (f_e) to predict the current state output y_e . In the whole loop of LSTM, previous information is utilized recursively. The input gate (i_e), forget gate (m_e) and the output gate (o_e) parameters of LSTM are defined as

$$i_e = \delta(W_i [h_{e-1}, f_e + \psi_i]) \quad (12)$$

$$m_e = \delta(W_m [h_{e-1}, f_e + \psi_m]) \quad (13)$$

$$o_e = \delta(W_o [h_{e-1}, f_e + \psi_o]) \quad (14)$$

where δ is the logistic sigmoid function, W is the weight matrix and ψ is the bias of each gate. Activation vector and hidden state can now be computed as

$$c_e = i_e \odot \tanh(W_c [h_{e-1}, f_e + \psi_c]) + m_e \odot c_{e-1} \quad (15)$$

$$h_e = o_e \odot \tanh(c_e) \quad (16)$$

where, the \odot represents the point wise multiplication. The final output of LSTM layer

$$y_e = W_y h_e + \psi_y \quad (17)$$

becomes the input to the Dense layer. The initial state parameter will be derived after model training for subsequent predictions. The output of the dense layer neurons could be given by equation (6) with LSTM layer output as the input. The kinematics parameters output can be obtained by the equation (9).

D. Hybrid Model II : WPD CNN-LSTM based

Reconstruction of hand movement profiles using low frequency EEG have been reported in 2D [25] and 3D spaces [26]. These results indicate that detailed limb kinematic information could be present in the low frequency components of EEG, and could be decoded using the proposed model. Therefore, an advanced version of CNN-LSTM based on wavelet packet decomposition is proposed that decompose

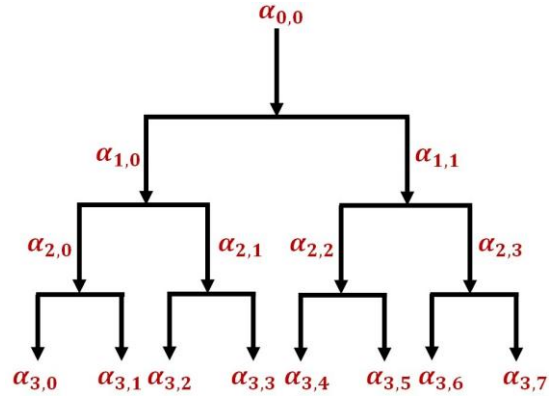


Fig. 8: Illustration of the three level wavelet packet decomposition.

the EEG signal into sub-bands with increasing resolution towards the lower frequency band. It may be noted from Fig. 6 that rather than utilising directly the pre-processed time domain EEG signal, wavelet coefficients of the EEG signal are utilized in hybrid model II by employing wavelet packet decomposition [27], [44]. The WPD, also known as optimal sub-band tree structuring, consists of a tree kind of structure with $a_{0,0}$ representing the root node or original signal of the tree as shown in Fig. 8. In the generalized node notation $a_{p,r}$, p denotes the scale and r denotes the sub-band index within the scale. The node $a_{p,r}$ can be decomposed into two orthogonal parts: an approximation space $a_{p,r}$ to $a_{p+1,2r}$ and detailed space $a_{p,r}$ to $a_{p+1,2r+1}$. This can be performed by dividing orthogonal basis $\{\theta_p(t - 2^p r)\}_{r \in \mathbb{Z}}$ of $a_{p,r}$ into two new orthogonal bases $\{\theta_{p+1}(t - 2^{p+1} r)\}_{r \in \mathbb{Z}}$ of $a_{p+1,2r}$ and $\{\phi_{p+1}(t - 2^{p+1} r)\}_{r \in \mathbb{Z}}$ of $a_{p+1,2r+1}$. The scaling function $\theta_{p,r}(t)$ and the wavelet function $\phi_{p,r}(t)$ are defined as

$$\theta_{p,r}(t) = \frac{1}{\sqrt{|2^p|}} \theta \left(\frac{t - 2^p r}{2^p} \right) \quad (18)$$

$$\phi_{p,r}(t) = \frac{1}{\sqrt{|2^p|}} \phi \left(\frac{t - 2^p r}{2^p} \right) \quad (19)$$

The dilation factor 2^p , also known as the scaling parameters, measures the degree of compression or scaling. On the other hand, the location parameters $2^p r$ determines the time location of the wavelet function. This method is repeated P times. Total number of samples in the original signal is taken to be T , where $P \leq \log_2 T$. This results in $P \times T$ coefficients. Therefore, at the level of resolution p , where $p = 1, 2, \dots, P$, the tree has T coefficients divided into 2^p coefficient blocks or crystals. In this work, Daubechies (db1) is selected as mother wavelet. Total 5 decomposition level are utilized for getting better frequency resolution. Thereafter, the same deep learning architecture of CNN-LSTM is utilized as discussed in Subsection IV-C.

WPD coefficients corresponding to approx 120 trials generated at each of the WPD tree subspaces are utilised as feature matrix. This is divided into three parts : (i) training data (70% of the total data), (ii) testing data (15% of the total data), and (iii) cross validation (15% of the total data).

TABLE I: PCC analysis of (a) mLR, (b) MLP, (c) CNN-LSTM model in different frequency bands. WPD CNN-LSTM correlation coefficient is presented in the end coloumn labeled as WPD.

Subject ID	Direction	Frequency Band												WPD
		Delta (0.5-3 Hz)			Theta (3-7 Hz)			Alpha (7-12 Hz)			Entire (0.5-12 Hz)			
		(a)	(b)	(c)	(a)	(b)	(c)	(a)	(b)	(c)	(a)	(b)	(c)	
1	x	0.28	0.83	0.85	0.25	0.78	0.83	0.12	0.54	0.52	0.40	0.80	0.87	0.86
	y	0.32	0.84	0.87	0.25	0.82	0.77	0.22	0.53	0.56	0.43	0.84	0.91	0.89
	z	0.13	0.53	0.80	0.11	0.51	0.61	0.06	0.30	0.24	0.12	0.61	0.81	0.84
2	x	0.32	0.71	0.83	0.23	0.56	0.80	0.23	0.54	0.57	0.38	0.77	0.83	0.84
	y	0.28	0.76	0.82	0.24	0.66	0.78	0.25	0.32	0.44	0.41	0.74	0.88	0.88
	z	0.29	0.53	0.78	0.31	0.53	0.62	0.09	0.15	0.26	0.21	0.58	0.76	0.79
3	x	0.30	0.81	0.86	0.32	0.61	0.82	0.23	0.46	0.51	0.46	0.79	0.92	0.91
	y	0.38	0.82	0.89	0.31	0.72	0.79	0.26	0.41	0.50	0.52	0.83	0.91	0.92
	z	0.31	0.64	0.80	0.32	0.63	0.60	0.12	0.21	0.24	0.25	0.64	0.82	0.86
4	x	0.37	0.83	0.88	0.40	0.78	0.70	0.26	0.64	0.53	0.44	0.82	0.86	0.87
	y	0.43	0.83	0.92	0.41	0.80	0.78	0.28	0.52	0.59	0.43	0.84	0.93	0.91
	z	0.17	0.74	0.78	0.15	0.64	0.65	0.12	0.25	0.23	0.20	0.71	0.82	0.85
5	x	0.48	0.81	0.87	0.36	0.75	0.77	0.26	0.53	0.49	0.46	0.84	0.87	0.88
	y	0.52	0.81	0.85	0.23	0.76	0.79	0.27	0.51	0.54	0.52	0.85	0.91	0.89
	z	0.32	0.64	0.74	0.22	0.67	0.61	0.16	0.23	0.10	0.28	0.74	0.81	0.83
Average	x	0.35	0.80	0.86	0.31	0.70	0.78	0.22	0.54	0.53	0.43	0.80	0.87	0.87
	y	0.39	0.81	0.87	0.29	0.75	0.78	0.26	0.46	0.53	0.46	0.82	0.91	0.90
	z	0.24	0.62	0.78	0.22	0.60	0.62	0.11	0.23	0.21	0.21	0.66	0.80	0.83

TABLE II: Comparison with state-of-the-art techniques.

References	Space	Variation in Load	Variation in SF	Decoding Method	Correlation (mean)
Robinson et. al [12]	2D	N.A.	N.A.	mLR	(0.60±0.07)
Korik et. al. [15]	3D	N.A.	N.A.	mLR	x=0.39, y=0.56, z=0.59
Sosnik et. al. [16]	3D	N.A.	N.A.	mLR	x=0.25, y=0.50, z=0.48
Model I	3D	Yes	Yes	MLP	x=0.80, y=0.82, z=0.66
Hybrid Model I	3D	Yes	Yes	CNN-LSTM	x=0.87, y=0.91, z=0.80
Hybrid Model II	3D	Yes	Yes	WPD CNN-LSTM	x=0.87, y=0.90, z=0.83

Note: Surface Friction (SF), Not Available (N.A.).

V. PERFORMANCE EVALUATION

Performance of the three proposed source aware deep learning models are compared with the state-of-the-art mLR technique. Effectiveness of the proposed framework is established using the Pearson correlation coefficient (PCC) evaluation metric. Additionally, hand trajectory estimation in 3D space is presented and compared with the ground truth trajectory.

A. Pearson Correlation Coefficient Analysis

Pearson correlation coefficient is a linear correlation coefficient that returns a value between -1 to +1. A -1, +1 and 0 PCC value means there is a strong negative, strong positive and zero correlation respectively. Pearson correlation coefficient between measured (A) and estimated (B) kinematic parameters of total samples T is expressed as

$$\Pi(A, B) = \frac{1}{T-1} \sum_{i=1}^T \frac{A_i - \mu_A}{\sigma_A} \frac{B_i - \mu_B}{\sigma_B} \quad (20)$$

where, μ_x and σ_x are the mean and standard deviation of x with $x \in \{B\}$. The PCC analysis for the various approaches to hand kinematics prediction utilizing EEG signal is presented in Table I for the 5 subjects from WAY-EEG-GAL dataset. The correlation is presented along the three directions x , y and z . The time-frequency distribution plot for the dataset in Fig. 3 suggests that the EEG frequency power is dominant up to the alpha band. Hence, the PCC analysis is presented in three different frequency bands (Delta, Theta, and Alpha). The correlation was additionally analysed for the entire frequency band. The result is presented for each subject individually along with the average behavior. WPD CNN-LSTM utilises the entire frequency spectrum. The three deep learning based models are compared with the state-of-the-art mLR approach. It may be noted that all the deep learning based models performs reasonably well when compared to mLR method for all the subjects and in all the direction. The low correlation in z direction for all the methods is attributed to short and transit movement along this direction. The performance of the hybrid model I (CNN-LSTM based) is

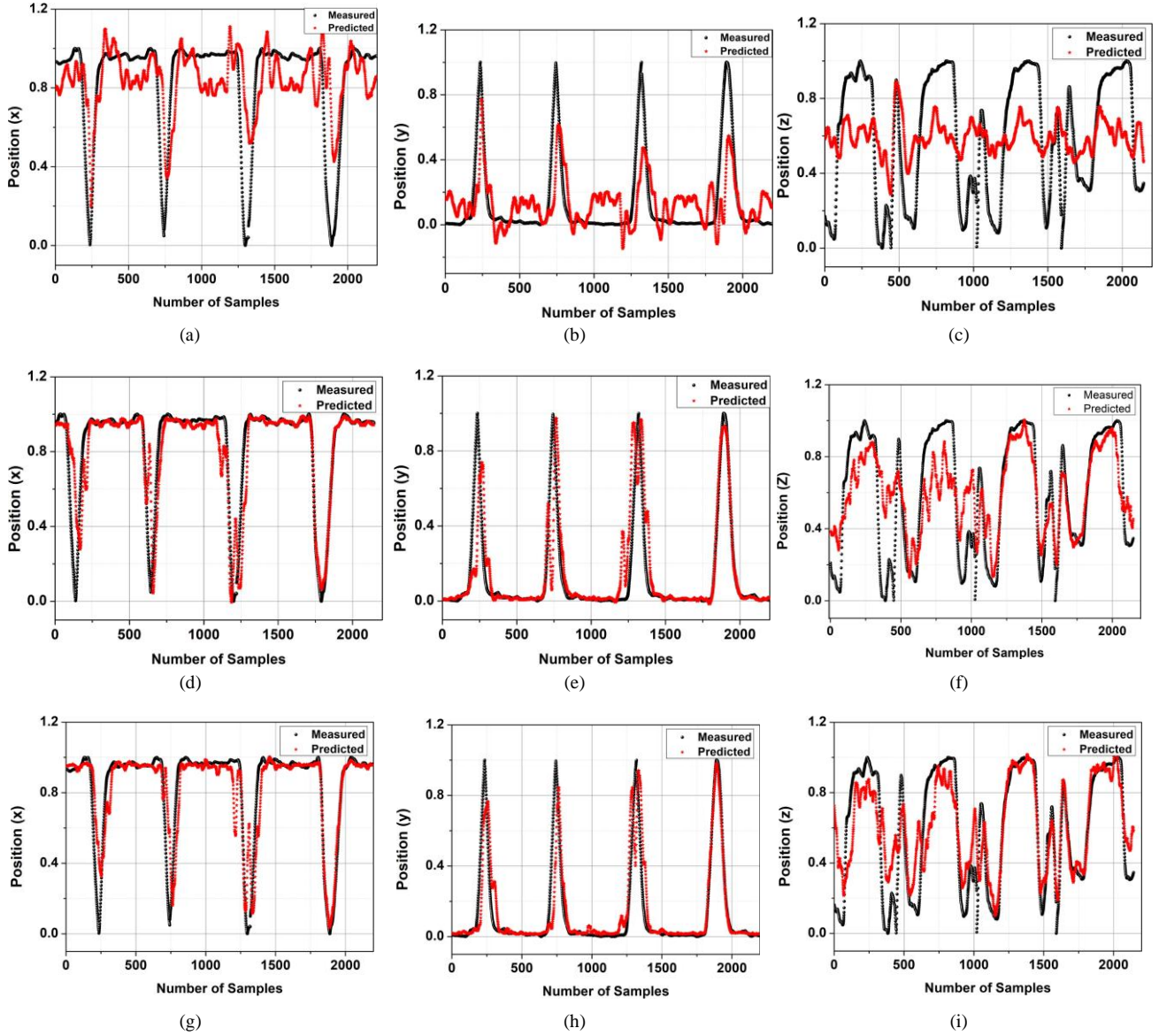


Fig. 9: Trajectory estimation in x, y and z direction using the mLR is presented in (a)-(c) respectively, the CNN-LSTM is presented in (d)-(f) respectively, and using the WPD CNN-LSTM is presented in (g)-(i) respectively.

seen to be better when compared to mLR and MLP techniques. The performance of the hybrid model II (WPD CNN-LSTM based) is similar to hybrid model I (CNN-LSTM based) along x and y directions. However, it outperforms all the methods in z direction, achieving higher correlation. Higher correlation in WPD based approach may be attributed to the fact that WPD decomposes the EEG signal into sub-bands with increasing resolution towards lower frequency band.

Source aware deep learning based models (MLP, CNN-LSTM and WPD CNN-LSTM) have been additionally compared with existing mLR variants [12], [15], [16]. The comparison is presented in Table II. The three deep learning based models shows superior performance when compared to the existing mLR variants. The utilised WAY-EEG-GAL dataset in the present study, additionally has higher complexity that includes different load variations and surface frictions (SF).

B. Trajectory Analysis

Comparative analysis of the true and predicted kinematic trajectories using existing and proposed approaches is presented herein. (x,y,z) coordinate location (or trajectory) of the subject's hand during the task is utilised as kinematic parameter. The measured and predicted trajectories of hand along x,y,z direction are plotted in Fig.9 (a)-(c) for mLR, Fig. 9 (d)-(f) for CNN-LSTM and Fig. 9 (g)-(i) for WPD CNN-LSTM. In CNN-LSTM model, lower trajectory mismatch is observed along the three x,y,z direction when compared to existing mLR technique. However, the two models suffers with greater trajectory mismatch in z direction. This is overcome in WPD CNN-LSTM model to a greater extent. Reasonably high correlation can be observed for all the three co-ordinates, making it more suitable for real-time application. The hand trajectory visualization of the true and estimated trajectory

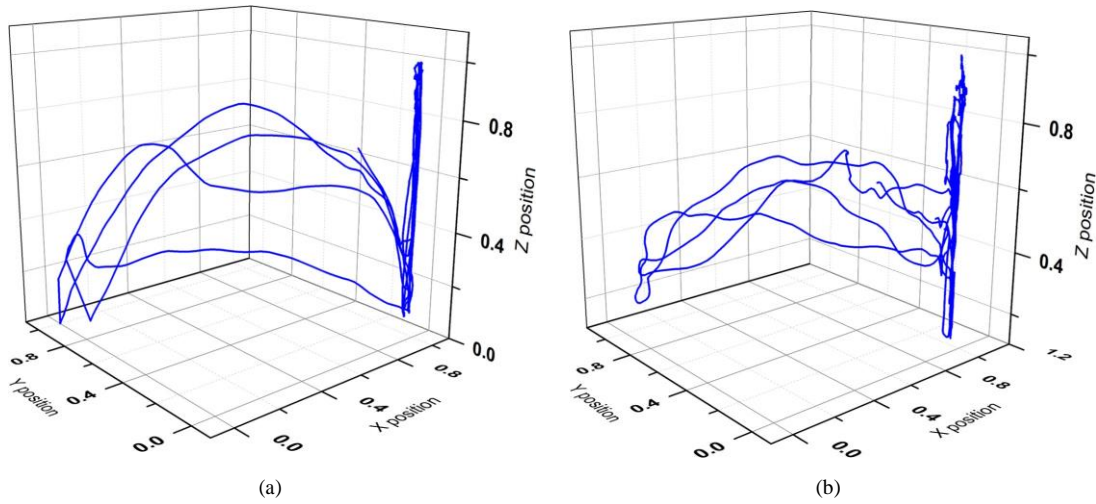


Fig. 10: Trajectory visualization in 3D space: (a) ground truth and (b) predicted trajectory from WPD CNN-LSTM method

from WPD CNN-LSTM method in 3D space is additionally, presented in Fig.10. True trajectory (Fig. 10 (a)) and predicted trajectory (Fig. 10 (b)) were observed to be nearly equivalent.

VI. CONCLUSION

In this work, source aware deep learning framework is proposed for hand kinematics parameter estimation from non-invasive EEG time series. In particular, MLP, CNN-LSTM and WPD CNN-LSTM models are proposed. An additional novelty of the work is to utilize brain source localization (using sLORETA) for motor intent mapping (channel selection) and accurate EEG time segment selection. Electrodes placed over the active brain region corresponding to the hand movement are utilized, rather than all the available sensors data for efficient computation. It has been observed that the EEG signal can provide the intended hand movement information approximately 300ms prior to actual hand movement. Early detection of intended hand movement is essential in communicating or controlling an external BCI devices. The performance of the proposed models are compared with the state-of-the-art mLR technique on the real GAL dataset. Effectiveness of the proposed framework is established using the Pearson correlation coefficient analysis. Additionally, hand trajectory estimation is presented and compared with the ground truth. Our proposed source aware deep learning models show significant improvement in correlation coefficient when compared with traditionally utilised mLR model. Our current study provides continuous decoding of brain activities that facilitate real time communication between the control block and the actuators block in BCI.

ACKNOWLEDGMENT

The authors would like to thank Prof. Shubhendu Bhasin, and Prof. Sushma Santapuri from Indian Institute of Technology Delhi (IITD), and Dr. Suriya Prakash from All India Institute of Medical Sciences (AIIMS) Delhi for their discussion and constructive comments during the preparation of the manuscript.

REFERENCES

- [1] D. Zhang, L. Yao, K. Chen, S. Wang, X. Chang, and Y. Liu, "Making sense of spatio-temporal preserving representations for EEG-based human intention recognition," *IEEE transactions on cybernetics*, vol. 50, no. 7, pp. 3033–3044, 2019.
- [2] N.-S. Kwak and S.-W. Lee, "Error correction regression framework for enhancing the decoding accuracies of ear-EEG brain-computer interfaces," *IEEE transactions on cybernetics*, vol. 50, no. 8, pp. 3654–3667, 2019.
- [3] Y. Zhang, C. S. Nam, G. Zhou, J. Jin, X. Wang, and A. Cichocki, "Temporally constrained sparse group spatial patterns for motor imagery BCI," *IEEE transactions on cybernetics*, vol. 49, no. 9, pp. 3322–3332, 2018.
- [4] J. Zhang, B. Wang, C. Zhang, Y. Xiao, and M. Y. Wang, "An EEG/EMG/EOG-based multimodal human-machine interface to real-time control of a soft robot hand," *Frontiers in neurobotics*, vol. 13, p. 7, 2019.
- [5] N. A. Bhagat, A. Venkatakrishnan, B. Abibullaev, E. J. Artz, N. Yozbatiran, A. A. Blank, J. French, C. Karmonik, R. G. Grossman, M. K. O'Malley *et al.*, "Design and optimization of an EEG-based brain machine interface (BMI) to an upper-limb exoskeleton for stroke survivors," *Frontiers in neuroscience*, vol. 10, p. 122, 2016.
- [6] W. He, Y. Zhao, H. Tang, C. Sun, and W. Fu, "A wireless BCI and BMI system for wearable robots," *IEEE Transactions on Systems, Man, and Cybernetics: Systems*, vol. 46, no. 7, pp. 936–946, 2015.
- [7] M. Deng, Z. Li, Y. Kang, C. P. Chen, and X. Chu, "A learning-based hierarchical control scheme for an exoskeleton robot in human-robot cooperative manipulation," *IEEE transactions on cybernetics*, vol. 50, no. 1, pp. 112–125, 2018.
- [8] Z. Gao, W. Dang, M. Liu, W. Guo, K. Ma, and G. Chen, "Classification of EEG Signals on VEP-Based BCI Systems With Broad Learning," *IEEE Transactions on Systems, Man, and Cybernetics: Systems*, 2020.
- [9] Y. Li, Q. Huang, Z. Zhang, T. Yu, and S. He, "An EEG-/EOG-Based Hybrid Brain-Computer Interface: Application on Controlling an Integrated Wheelchair Robotic Arm System," *Frontiers in Neuroscience*, vol. 13, p. 1243, 2019.
- [10] R. Alazrai, H. Alwanni, and M. I. Daoud, "EEG-based BCI system for decoding finger movements within the same hand," *Neuroscience letters*, vol. 698, pp. 113–120, 2019.
- [11] L. He, D. Hu, M. Wan, Y. Wen, K. M. Von Deneen, and M. Zhou, "Common Bayesian network for classification of EEG-based multiclass motor imagery BCI," *IEEE Transactions on Systems, Man, and Cybernetics: Systems*, vol. 46, no. 6, pp. 843–854, 2015.
- [12] N. Robinson, C. Guan, and A. Vinod, "Adaptive estimation of hand movement trajectory in an EEG based brain-computer interface system," *Journal of neural engineering*, vol. 12, no. 6, p. 066019, 2015.

- [13] N. Shajil, S. Mohan, P. Srinivasan, J. Arivudaiyanambi, and A. A. Murrugesan, "Multiclass Classification of Spatially Filtered Motor Imagery EEG Signals Using Convolutional Neural Network for BCI Based Applications," *Journal of Medical and Biological Engineering*, pp. 1–10, 2020.
- [14] R. M. Rangayyan, *Biomedical signal analysis*. John Wiley & Sons, 2015.
- [15] A. Korik, R. Sosnik, N. Siddique, and D. Coyle, "Decoding imagined 3D hand movement trajectories from EEG: evidence to support the use of mu, beta, and low gamma oscillations," *Frontiers in neuroscience*, vol. 12, p. 130, 2018.
- [16] R. Sosnik and O. B. Zur, "Reconstruction of hand, elbow and shoulder actual and imagined trajectories in 3D space using EEG slow cortical potentials," *Journal of Neural Engineering*, vol. 17, no. 1, p. 016065, 2020.
- [17] X. Liu, L. Jiao, L. Li, L. Cheng, F. Liu, S. Yang, and B. Hou, "Deep Multiview Union Learning Network for Multisource Image Classification," *IEEE Transactions on Cybernetics*, 2020.
- [18] T. Zhang, W. Zheng, Z. Cui, Y. Zong, and Y. Li, "Spatial-temporal recurrent neural network for emotion recognition," *IEEE transactions on cybernetics*, vol. 49, no. 3, pp. 839–847, 2018.
- [19] J. Zhang, C. Zong *et al.*, "Deep Neural Networks in Machine Translation: An Overview," *IEEE Intell. Syst.*, vol. 30, no. 5, pp. 16–25, 2015.
- [20] D. Borra, S. Fantozzi, and E. Magosso, "Interpretable and lightweight convolutional neural network for EEG decoding: Application to movement execution and imagination," *Neural Networks*, 2020.
- [21] Y. Sun, B. Xue, M. Zhang, G. G. Yen, and J. Lv, "Automatically designing CNN architectures using the genetic algorithm for image classification," *IEEE transactions on cybernetics*, vol. 50, no. 9, pp. 3840–3854, 2020.
- [22] S. Yang, W. Wang, C. Liu, and W. Deng, "Scene understanding in deep learning-based end-to-end controllers for autonomous vehicles," *IEEE Transactions on Systems, Man, and Cybernetics: Systems*, vol. 49, no. 1, pp. 53–63, 2018.
- [23] S. U. Amin, M. Alsulaiman, G. Muhammad, M. A. Mekhtiche, and M. S. Hossain, "Deep Learning for EEG motor imagery classification based on multi-layer CNNs feature fusion," *Future Generation computer systems*, vol. 101, pp. 542–554, 2019.
- [24] J. Du, C.-M. Vong, and C. P. Chen, "Novel efficient RNN and LSTM-like architectures: Recurrent and gated broad learning systems and their applications for text classification," *IEEE transactions on cybernetics*, 2020.
- [25] A. Presacco, R. Goodman, L. Forrester, and J. L. Contreras-Vidal, "Neural decoding of treadmill walking from noninvasive electroencephalographic signals," *Journal of neurophysiology*, vol. 106, no. 4, pp. 1875–1887, 2011.
- [26] T. J. Bradberry, R. J. Gentili, and J. L. Contreras-Vidal, "Reconstructing three-dimensional hand movements from noninvasive electroencephalographic signals," *Journal of Neuroscience*, vol. 30, no. 9, pp. 3432–3437, 2010.
- [27] Y. Zhang, B. Liu, X. Ji, and D. Huang, "Classification of EEG signals based on autoregressive model and wavelet packet decomposition," *Neural Processing Letters*, vol. 45, no. 2, pp. 365–378, 2017.
- [28] M. T. Sadiq, X. Yu, Z. Yuan, Z. Fan, A. U. Rehman, G. Li, and G. Xiao, "Motor imagery EEG signals classification based on mode amplitude and frequency components using empirical wavelet transform," *IEEE Access*, vol. 7, pp. 127 678–127 692, 2019.
- [29] M. D. Luciw, E. Jarocka, and B. B. Edin, "Multi-channel EEG recordings during 3,936 grasp and lift trials with varying weight and friction," *Scientific data*, vol. 1, no. 1, pp. 1–11, 2014.
- [30] R. Grech, T. Cassar, J. Muscat, K. P. Camilleri, S. G. Fabri, M. Zervakis, P. Xanthopoulos, V. Sakkalis, and B. Vanrumste, "Review on solving the inverse problem in EEG source analysis," *Journal of neuroengineering and rehabilitation*, vol. 5, no. 1, p. 25, 2008.
- [31] A. Giri, L. Kumar, and T. Gandhi, "Head Harmonics Based EEG Dipole Source Localization," in *2019 53rd Asilomar Conference on Signals, Systems, and Computers*. IEEE, 2019, pp. 2149–2153.
- [32] J. C. Mosher, P. S. Lewis, and R. M. Leahy, "Multiple dipole modeling and localization from spatio-temporal MEG data," *IEEE Transactions on Biomedical Engineering*, vol. 39, no. 6, pp. 541–557, 1992.
- [33] A. Giri, L. Kumar, and T. K. Gandhi, "Brain source localization in head harmonics domain," *IEEE Transactions on Instrumentation and Measurement*, vol. 70, pp. 1–10, 2020.
- [34] S. Baillet, J. C. Mosher, and R. M. Leahy, "Electromagnetic brain mapping," *IEEE Signal Processing Magazine*, vol. 18, no. 6, pp. 14–30, Nov 2001.
- [35] K. Uutela, M. Hamalainen, and R. Salmelin, "Global optimization in the localization of neuromagnetic sources," *IEEE Transactions on Biomedical Engineering*, vol. 45, no. 6, pp. 716–723, 1998.
- [36] M. S. Hämäläinen, "Interpreting measured magnetic fields of the brain: Estimates of current distributions," *Univ. Helsinki, Finland Tech. Rep. TKK-F-A559*, 1984.
- [37] M. S. Hämäläinen and R. J. Ilmoniemi, "Interpreting magnetic fields of the brain: minimum norm estimates," *Medical and biological engineering and computing*, vol. 32, no. 1, pp. 35–42, 1994.
- [38] R. D. Pascual-Marqui, D. Lehmann, T. Koenig, K. Kochi, M. C. Merlo, D. Hell, and M. Koukkou, "Low resolution brain electromagnetic tomography (LORETA) functional imaging in acute, neuroleptic-naïve, first-episode, productive schizophrenia," *Psychiatry Research: Neuroimaging*, vol. 90, no. 3, pp. 169–179, 1999.
- [39] R. D. Pascual-Marqui *et al.*, "Standardized low-resolution brain electromagnetic tomography (sLORETA): technical details," *Methods Find Exp Clin Pharmacol*, vol. 24, no. Suppl D, pp. 5–12, 2002.
- [40] C.-T. Lin, C.-H. Chuang, Y.-C. Hung, C.-N. Fang, D. Wu, and Y.-K. Wang, "A driving performance forecasting system based on brain dynamic state analysis using 4-D convolutional neural networks," *IEEE transactions on cybernetics*, 2020.
- [41] A. Narang, B. Batra, A. Ahuja, J. Yadav, and N. Pachauri, "Classification of EEG signals for epileptic seizures using Levenberg-Marquardt algorithm based Multilayer Perceptron Neural Network," *Journal of Intelligent & Fuzzy Systems*, vol. 34, no. 3, pp. 1669–1677, 2018.
- [42] S. Hochreiter and J. Schmidhuber, "Long short-term memory," *Neural computation*, vol. 9, no. 8, pp. 1735–1780, 1997.
- [43] X. Ma, D. Wang, D. Liu, and J. Yang, "DWT and CNN based multi-class motor imagery electroencephalographic signal recognition," *Journal of Neural Engineering*, vol. 17, no. 1, p. 016073, 2020.
- [44] R. N. Khushaba, S. Kodagoda, S. Lal, and G. Dissanayake, "Driver drowsiness classification using fuzzy wavelet-packet-based feature-extraction algorithm," *IEEE transactions on biomedical engineering*, vol. 58, no. 1, pp. 121–131, 2010.